Available online at www.sciencedirect.com
ScienceDirect
Applied Catalysis B: Environmental 73 (2007) 336–344
APPLIED CATALYSIS B: ENVIRONMENTAL
www.elsevier.com/locate/apcatb

Syngas production from butane using a flame-made $Rh/Ce_{0.5}Zr_{0.5}O_2$ catalyst

Nico Hotz [a], Michael J. Stutz [a], Stefan Loher [b], Wendelin J. Stark [b], Dimos Poulikakos [a,*]

[a] *Laboratory of Thermodynamics in Emerging Technologies, Institute of Energy Technology, Department of Mechanical and Process Engineering, ETH Zurich, CH-8092 Zurich, Switzerland*

[b] *Functional Materials Laboratory, Institute for Chemical and Bioengineering, Department of Chemistry and Applied Biosciences, ETH Zurich, CH-8092 Zurich, Switzerland*

Received 20 September 2006; received in revised form 1 January 2007; accepted 5 January 2007
Available online 12 January 2007

Abstract

The capability of flame-made $Rh/Ce_{0.5}Zr_{0.5}O_2$ nanoparticles catalyzing the production of H_2- and CO-rich syngas from butane was investigated for different Rh loadings (0–2.0 wt% Rh) and two different ceramic fibers (Al_2O_3/SiO_2 and SiO_2) as plugging material in a packed bed reactor for a temperature range from 225 to 750 °C. The main goal of this study was the efficient processing of butane at temperatures between 500 and 600 °C for a micro-intermediate-temperature SOFC system. Our results showed that $Rh/Ce_{0.5}Zr_{0.5}O_2$ nanoparticles offer a very promising material for butane-to-syngas conversion with complete butane conversion and a hydrogen yield of 77% at 600 °C. The catalytic performance of packed beds strongly depended on the use of either Al_2O_3/SiO_2 or SiO_2 fiber plugs. This astonishing effect could be attributed to the interplay of homogeneous and heterogeneous chemical reactions during the high-temperatures within the reactor.

Keywords: Butane processing; Syngas; Catalytic nanoparticles; Rhodium catalyst; Micro-reactor; Fuel cell; Intermediate-temperature SOFC

1. Introduction

A promising application of fuel cells are miniaturized fuel cell systems generating electric power of the order of a few watts to power small portable electronic devices such as laptops, cameras, and cell phones. Small fuel cell systems using hydrocarbons as a fuel combine the high energetic efficiency of fuel cells with the high availability and easy storage of hydrocarbon fuels [1]. Modern materials for solid oxide fuel cells (SOFCs) lead to higher efficiencies compared to other types of fuel cells at intermediate operating temperatures, namely in the range of 500 and 600 °C [2–4]. An important benefit of SOFCs is the possibility of using hydrogen (H_2) and carbon monoxide (CO) simultaneously for electricity production, whereas low temperature fuel cells cannot convert CO or even suffer from CO poisoning. This aspect is particularly interesting when fuel cells are supplied with reformate feeds from a hydrocarbon processor which always contain significant amounts of CO. An interesting hydrocarbon fuel for this application is butane, allowing high efficiency for the production of a H_2- and CO-rich syngas at moderate temperature similar to the mentioned intermediate temperature of modern SOFCs. Butane can be stored relatively easily in liquid phase at room temperature and low pressure and is widely available.

The major goal of this study was to investigate the feasibility of butane-to-syngas conversion with high H_2 and CO mole fractions at relatively low temperatures, while obeying strict limitations of space considering the application of a micro-SOFC system. To achieve these demanding requirements, ceria/zirconia nanoparticles with rhodium doping ($Rh/Ce_{0.5}Zr_{0.5}O_2$) made by flame spray synthesis were used as catalysts. Nanoparticles provide open and easily accessible catalytically active surfaces with a high surface-to-volume ratio, as shown by Stark et al. [5]. Zirconia contributes to the thermal stability of the nanoparticles and ceria offers optimal properties for

* Corresponding author. Tel.: +41 44 632 2738; fax: +41 44 632 1176.
E-mail address: dimos.poulikakos@ethz.ch (D. Poulikakos).

0926-3373/$ – see front matter © 2007 Elsevier B.V. All rights reserved.
doi:10.1016/j.apcatb.2007.01.001

Nomenclature

GSV	gas space velocity (s^{-1})
$\dot{n}$	molar flow rate (mol s^{-1})
S_{CO}	carbon monoxide selectivity
S_{H_2}	hydrogen selectivity
t_{space}	space time (s)
V	volume (m^3)
$\dot{V}$	volumetric flow rate (m^3 s^{-1})
X	mole fraction
Greek letters	
η	butane conversion
ϕ	equivalence or C/O ratio
ψ	hydrogen yield

oxygen exchange on the particle surface [6]. The catalytic performance of these nanoparticles was analyzed in a mini packed bed reactor. A desirable reaction path for syngas production from hydrocarbons is partial oxidation (POX), written as

$$C_4H_{10} + 2O_2 \rightarrow 5H_2 + 4CO, \quad (1)$$

which achieves high yields of H_2 and CO. Another effective reaction for hydrocarbon processing is steam reforming (SR), where butane reacts with water:

$$C_4H_{10} + 4H_2O \rightarrow 9H_2 + 4CO. \quad (2)$$

A second water consuming reaction which might take place in a micro-reactor besides SR is water gas shift (WGS):

$$CO + H_2O \rightarrow H_2 + CO_2. \quad (3)$$

A well performing butane processor should show high selectivity towards POX products instead of total oxidation (TOX) products of butane:

$$C_4H_{10} + 6.5O_2 \rightarrow 5H_2O + 4CO_2. \quad (4)$$

Another objective of this study was the investigation of the effect of different plugging materials of the packed bed on the catalytic performance. Ceramic fibers made of silicon oxide and aluminum oxide (Al_2O_3/SiO_2), which is widely used as the sealing material and the substrate of monoliths or foams in hydrocarbon-to-hydrogen reactors, e.g. [7–11], and pure SiO_2 were used to form plugs.

An important aspect of catalytic hydrocarbon processors is the combination of homogeneous and heterogeneous reactions simultaneously taking place. Previous studies [12–14] have suggested that oxidative dehydrogenation of propane is a combination of gas-phase homogeneous and catalyzed heterogeneous reactions, where Xu and Lundsford [14] based this interpretation on experiments with SiO_2 chips comparable to our SiO_2-sand filled tubes. Huff and Schmidt [15] showed that oxidative dehydrogenation of butane in short-time reactors was highly affected by an increase of reactor surface in the absence of noble metal catalysts. Lemonidou and Stambouli [16] confirmed this effect of the surface-to-volume ratio on oxidative dehydrogenation of butane in a non-catalytic SiO_2 reactor. The triggering of gas-phase homogeneous reactions by radicals formed by surface reactions during catalytic POX of methane was reported by Campbell et al. [17] and of propane by Silberova et al. [18] and Aartun et al. [19]. The same finding for POX of butane was reported by Marengo et al. [20]. The latter suggested that fast ignition of exothermic homogeneous reactions by the surface of inert packing material such as SiO_2 was possible in absence of noble metal catalysts during POX of butane.

The conversion of hydrocarbons to syngas by POX is usually accompanied by TOX followed by SR and WGS, which produce H_2 and CO as well. This indirect reaction mechanism was already suggested by Kunimori et al. for butane on platinum [21]. More recently, this autothermal reforming path was investigated by Wang and Gorte for hydrocarbons on Pd/ceria [22]. These studies suggested ceria-supported precious metals as well-suitable catalysts for hydrocarbon reforming catalyzing POX, SR, and WGS simultaneously.

2. Experiments

2.1. Catalyst preparation

$Ce_{0.5}Zr_{0.5}O_2$ nanoparticles with optional rhodium doping were prepared in a one-step process by flame spray synthesis described by Madler et al. and Stark et al. [23,24]. For the ceria/zirconia precursor, cerium(III) 2-ethylhexanoate (12 wt% Ce, Shepherd Chemical Company) and zirconium(IV) 2-ethylhexanoate (18 wt% Zr, Borchers GmbH) were mixed to result in a metal molar ratio Ce/Zr of 1:1 and diluted with xylene to a total metal concentration of 0.8 mol L^{-1}. Rhodium(III) 2-ethylhexanoate (UMICORE AG & Co.) was optionally added to the Ce/Zr-precursor such that the calculated rhodium content in the ternary system Rh/ceria/zirconia ($Rh/Ce_{0.5}Zr_{0.5}O_2$) was 2.0, 0.5, 0.25, and 0.1 wt%. The mixtures were fed (5 mL min^{-1}) through a capillary (i.d. 0.4 mm) using a gear-ring pump (HNP Microsysteme) and were dispersed by oxygen at the tip of the capillary (5 L min^{-1}, constant pressure drop at the nozzle 1.5 bar, PanGas, tech) following ignition by a methane (1.13 L min^{-1}, PanGas, tech)/oxygen (2.41 L min^{-1}, PanGas, tech) supporting flame. The burning spray of the flame synthesis reactor was stabilized by a concentric oxygen sheath flow (230 L h^{-1}, PanGas, tech). All gas flows were controlled by calibrated mass flow controllers (Brooks). The particles formed in the flame were separated from the off-gas with a glass fiber filter (Whatman GF/A, 25.7 cm in diameter) placed above the flame by the aid of a vacuum pump (Busch Seco SV 1040C). The thermal stability was tested by sintering as prepared particles at 1000 °C for 16 h, under air, using a heating rate of 10 °C min^{-1} and measuring the remaining specific surface area.

2.2. Catalyst characterization

The specific surface area (SSA) of the powders was measured by nitrogen adsorption at 77 K on a Micromeritics

Tristar using the BET method (error ±3%). The phase composition and formation of ceria/zirconia mixed oxides was investigated by X-ray powder diffraction on a Stoe STADI-P2 (Ge monochromator, Cu $K\alpha_1$, PSD detector). To determine the rhodium content, powders were digested in hydrochloric acid (37 wt%, J.T. Baker) and analyzed by flame atomic absorption spectrometry (AAS) on a Varian SpectrAA 220FS (slit width 0.2 nm, lamp current 5.0 mA) applying a N_2O (11.0 L min^{-1}, PanGas)/acetylene (6.23 L min^{-1}, PanGas) flame and measuring absorption at a wavelength of 369.2 nm [25]. Transmission electron micrographs were recorded on a CM30 ST (Philips, LaB_6 cathode, operated at 300 kV, point resolution ~2 Å). Prior to analysis, the particles were dispersed in ethanol and deposited onto a carbon foil supported on a copper grid.

2.3. Test setup for catalyst performance measurements

Expanded butane from a liquid tank (PanGas, 3.5, 99.95%) at 2.5 bar was mixed with compressed synthetic air (79% N_2, 21% O_2, PanGas, 5.6, purity of both species: 99.9999%) from a gas tank (Fig. 1). Both flow rates were controlled by Low Delta-P flow meters (Bronckhorst). The flow meters allowed control of the inlet pressure to reach the ambient pressure at the system outlet, such as to be able to operate the reactor slightly above ambient pressure. The butane/air mixture was fed into a packed bed reactor inside an Inconel tube (Alloy 600, i.d. 2 mm) and heated by a tube furnace (MTF 12/38/250, Carbolite). The tube was heated over a length of 30 cm, ensuring isothermal conditions along the packed bed reactor (total length: 11 mm) placed in the middle of the furnace. The assumption of isothermal conditions in the reactor was confirmed by temperature measurements in the packed bed, shown in Appendix A. The product gas leaving the furnace through an Inconel tube was maintained at around 115 °C to avoid condensation of H_2O. The gas composition was analyzed by a gas chromatograph (6890 GC) coupled with a mass spectrometer (5975 MS, Agilent), using a HP-MOLSIV and a HP-PlotQ column (Agilent), respectively. Helium (PanGas, 5.6, 99.9996%) was added as an internal standard for GC calibration. Under typical run conditions, the molar product gas balances of C, H, and O were closed within 5%.

The packed bed consisted of 22.5 mg purified and calcined SiO_2 sand (Riedel-deHaën, average diameter: 0.2 mm) and 7.5 mg $Rh/Ce_{0.5}Zr_{0.5}O_2$ nanoparticles (0–2.0 wt% Rh), prepared as shown before and homogenously distributed onto the sand particles. For reference measurements without nanoparticles, packed beds with 30.0 mg SiO_2 were prepared. These porous packed beds were fixed in the Inconel tube between ceramic fiber plugs, as shown in Fig. 1. In order to investigate the reactivity of the fibers, two different ceramic materials were used: ceramic fiber paper made of SiO_2 and Al_2O_3 (1:1, CT 1260 P, Contherm, mean fiber diameter: approximately 18 μm, mean fiber length: 5 mm) or pure SiO_2 fibers (Riedel-deHaën, mean fiber diameter: 16 μm, mean fiber length: 5 mm). The catalytic effect of the Inconel tube on the reactions was negligible in presence of $Rh/Ce_{0.5}Zr_{0.5}O_2$ catalyst, as proven by a comparison with a packed bed in a quartz tube (see Appendix A).

2.4. Testing procedures

The activity of $Rh/Ce_{0.5}Zr_{0.5}O_2$ catalysts was tested at constant air and butane inlet flow rates of 15.0 and 1.2 mL min^{-1}, respectively, leading to mole fractions of $X_{C_4H_{10}} = 7.4\%$, $X_{O_2} = 18.5\%$, and $X_{N_2} = 74.1\%$. This corresponded to a butane mass flow of 0.2 g h^{-1}. The C/O ratio or equivalence ratio ϕ based on POX was defined as

$$\phi = 2\frac{\dot{n}_{C_4H_{10},in}}{\dot{n}_{O_2,in}} \quad (5)$$

and was kept constant at $\phi = 0.8$ for all measurements, as suggested by previous numerical studies on micro-hydrocarbon processors [26,27]. The entire reactor was heated from 225 to 750 °C at a heating rate of 2.5 °C min^{-1} under air/butane flow. The molar composition of the outlet gas was determined every 75 °C. The gas space velocity (GSV) was defined as the ratio of total volumetric flow rate at the reactor inlet and reactor volume:

$$\mathrm{GSV} = \frac{\dot{V}_{gas,in}}{V_{reactor}} = \frac{1}{t_{space}}, \quad (6)$$

which is the reciprocal of the space time t_{space} [28]. The mean gas velocity at the reactor inlet varied from 0.14 to 0.29 m s^{-1}, depending on the reactor temperature, leading to GSV between 15.7 and 32.3 s^{-1} and t_{space} in the range of 63.7 and 31.0 ms. Based on the results of the GC/MS, the butane conversion η of the micro-reactor was determined as the molar ratio between converted butane and inlet butane:

$$\eta = \frac{\dot{n}_{C_4H_{10},in} - \dot{n}_{C_4H_{10},out}}{\dot{n}_{C_4H_{10},in}}. \quad (7)$$

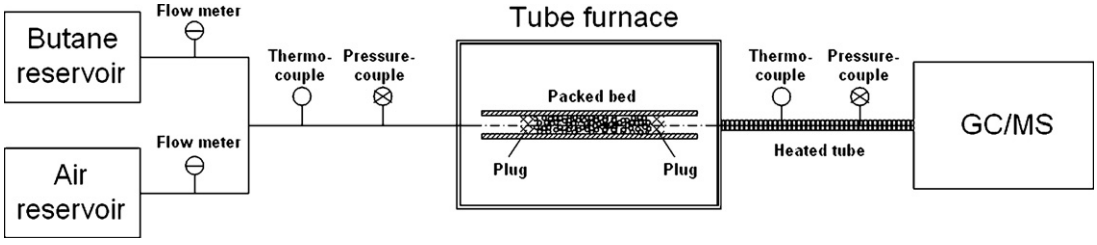

Fig. 1. Schematic of the test setup for catalyst performance measurements of a packed bed reactor.

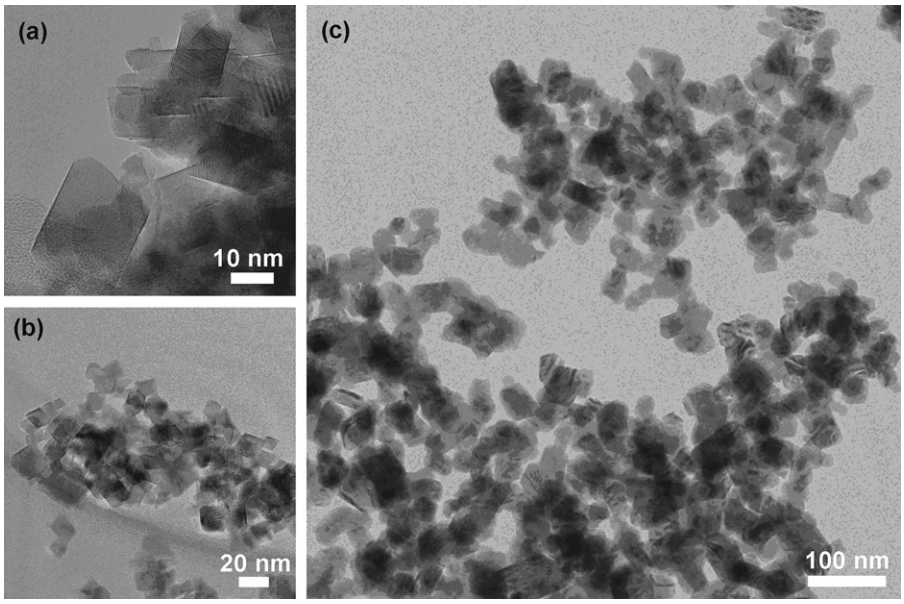

Fig. 2. Electron micrographs of flame-made $Ce_{0.5}Zr_{0.5}O_2$ (a) and 0.5 wt% $Rh/Ce_{0.5}Zr_{0.5}O_2$ (b) showed regularly shaped nanoparticles with similar morphology. After sintering at 1000 °C for 16 h under air, the $Rh/Ce_{0.5}Zr_{0.5}O_2$ (c) displayed marginal particle growth. Sintering necks between adjacent particles stabilized the open, well accessible material.

The hydrogen yield was defined as the molar ratio of H_2 in the outlet gas and the maximal possible amount of H_2 formed at full conversion according to Eq. (1):

$$\psi = \frac{\dot{n}_{H_2,out}}{5\dot{n}_{C_4H_{10},in}}. \quad (8)$$

The selectivities for H_2 and CO were defined as

$$S_{H_2} = \frac{\dot{n}_{H_2,out}}{\dot{n}_{H_2,out} + \dot{n}_{H_2O,out}} \quad (9)$$

and

$$S_{CO} = \frac{\dot{n}_{CO,out}}{\dot{n}_{CO,out} + \dot{n}_{CO_2,out}}. \quad (10)$$

3. Results

3.1. Catalyst characterization

Feeding mixtures of rhodium, cerium, and zirconium carboxylate precursors into a flame spray synthesis unit allowed for continuous production of ceria/zirconia nanoparticles with optional rhodium doping (nominal content 0.5 wt% Rh) at a nominal production rate of 43 g/h. Transmission electron microscope (TEM) images of as-prepared ceria/zirconia $Ce_{0.5}Zr_{0.5}O_2$ (Fig. 2a) and 0.5 wt% $Rh/Ce_{0.5}Zr_{0.5}O_2$ (Fig. 2b) showed highly regular, crystalline, sharp-edged nanoparticles of 10–40 nm. Addition of 0.5 wt% Rh had no significant influence on the morphology. No metallic rhodium particles could be detected in electron micrographs (TEM) or by energy dispersive X-ray analysis (not shown) indicating a high dispersion of rhodium on the support material. This stays in line with previous studies on Pd/alumina [29], Pt/alumina [30], and Pt/ceria/zirconia [31] synthesized by flame spray pyrolysis that also reported high noble metal dispersions. Both as-prepared materials exhibited a high BET specific surface area (SSA) of 103 $m^2\,g^{-1}$ for $Ce_{0.5}Zr_{0.5}O_2$ and 106 $m^2\,g^{-1}$ for 0.5 wt% $Rh/Ce_{0.5}Zr_{0.5}O_2$. The Rh content of the as-prepared samples was measured by flame atomic absorption spectrometry (AAS). Ceria/zirconia contained less than 0.002 wt% Rh (error of measurement) and 0.51 wt% Rh for the doped material, confirming that no Rh was lost during synthesis.

Severe sintering conditions (1000 °C for 16 h [31]) resulted in some sintering but corroborated the high thermal stability of flame-made CeO_2/ZrO_2 (Fig. 2c), which corresponds well with results of Stark et al. [24]. Sintered samples showed specific surface areas of 28 $m^2\,g^{-1}$ ($Ce_{0.5}Zr_{0.5}O_2$) and 22 $m^2\,g^{-1}$

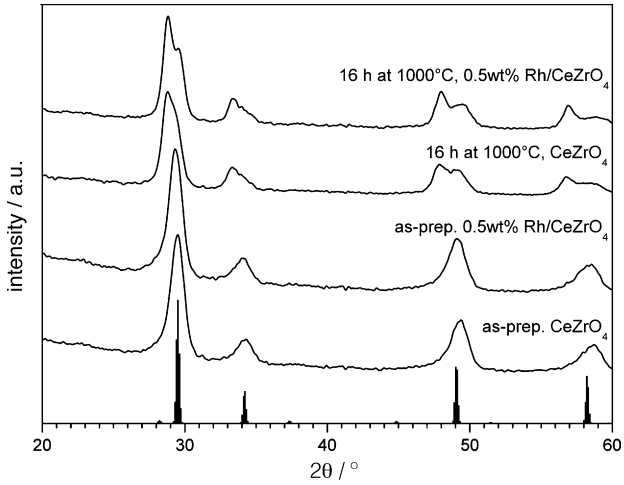

Fig. 3. X-ray diffraction patterns of as-prepared (bottom) and sintered samples (top). After preparation, the material consisted of a homogenous ceria/zirconia solid solution. The severe sintering conditions resulted in partial phase segregation. Bottom: reference pattern of κ-$Ce_{0.5}Zr_{0.5}O_2$ [32].

(0.5 wt% $Rh/Ce_{0.5}Zr_{0.5}O_2$). In contrast to studies on Pt/alumina [30] and Pt/ceria/zirconia [31], rhodium had a small influence on the sintering of the support material.

The phase composition of as-prepared or sintered samples was measured by X-ray diffraction (XRD) (Fig. 3). Both powders showed broad signals after preparation which could be attributed to a solid solution of cubic metastable κ-$Ce_{0.5}Zr_{0.5}O_2$ [32] as observed in previous studies on flame-made ceria/zirconia nanoparticles [24,31,33]. The Rh containing $Ce_{0.5}Zr_{0.5}O_2$ exhibited no additional reflections of the metallic phase, which stays in agreement to the electron micrographs (Fig. 2). After sintering of the nanoparticles, signals for cubic CeO_2 [34] evolved next to the solid solution and were attributed to partial phase separation [24].

3.2. Influence of Al_2O_3/SiO_2 and SiO_2 fiber plugs on the syngas production

In Fig. 4, the syngas production of packed bed reactors containing Al_2O_3/SiO_2 fiber plugs is compared to that of packed bed reactors containing SiO_2 plugs. For packed bed reactors consisting of SiO_2 sand and ceramic fiber plugs without any $Rh/Ce_{0.5}Zr_{0.5}O_2$ catalyst, the conversion of butane started above 400 °C (Fig. 4a). Between 500 and 700 °C, the butane conversion was significantly higher for pure SiO_2 fibers than for Al_2O_3/SiO_2 fibers. Without catalyst, the amount of produced CO was very low and a small amount of H_2 was only produced at 750 °C (not shown here). For reactors containing $Ce_{0.5}Zr_{0.5}O_2$ nanoparticles with 0.5 wt% Rh, conversion of butane started below 300 °C (Fig. 4a). Between 300 and 400 °C, the butane conversion was slightly higher when Al_2O_3/SiO_2 fiber plugs were used. However, Al_2O_3/SiO_2 fibers led to stagnation in butane conversion (at around 50%) up to 525 °C, compared to a significantly higher conversion for pure SiO_2 fibers with up to 99% at 750 °C. The H_2 production grew with increasing the reactor temperature up to 375 °C, stagnated between 375 and 500 °C for Al_2O_3/SiO_2 fibers, and finally increased again for temperatures up to 750 °C, as it can be seen from the hydrogen yield ψ (Fig. 4a) and the H_2 selectivity S_{H_2} (Fig. 4b). For SiO_2 fibers, no stagnation occurred at intermediate temperatures and the H_2 production exceeded evidently those of Al_2O_3/SiO_2. The CO production started above 300 °C and for SiO_2, it rose rapidly to a CO selectivity S_{CO} of 73% at 675 °C and 79% at 750 °C (Fig. 4b). For Al_2O_3/SiO_2 fibers, the CO production increased slower with temperature, reaching high CO selectivities only above 675 °C.

There were no significant amounts of lower hydrocarbons in the product gas detected. In presence of $Rh/Ce_{0.5}Zr_{0.5}O_2$ catalysts, the mole fractions of lower hydrocarbons were negligible (always below 0.05%), except for methane, which was below 0.7% for Al_2O_3/SiO_2 fibers and below 0.3% for SiO_2 fibers. For the measurement without any catalytical nanoparticles, the ethane and propane mole fractions were below 0.05% and the ethylene and propylene mole fractions below 0.1%. The methane mole fraction was below 0.9% for this case. Therefore, it can be concluded that in the absence of an $Rh/Ce_{0.5}Zr_{0.5}O_2$ catalyst even lower hydrocarbons were formed, but their amount was still insignificant.

The molar product gas balance of C closed within 1% for all measurements, indicating that no significant carbon deposition took place inside the reactor. The occurrence of carbon deposition was also tested by optical inspection. The amount of 0.1 mg of carbon mixed with packed beds (22.5 mg SiO_2 sand and 7.5 mg nanoparticles with different Rh loadings) can be optically inspected. For all examined packed beds, no change of color after one measurement cycle (around 400 min) could be detected. Measurement of the weight of the packed bed before and after runs did not indicate the deposition of significant amounts of carbon (detection limit: 0.1 mg, corresponding to 3.3 mg C per g packed bed material).

For both packed beds containing catalyst, complete conversion of O_2 could be detected for temperatures above 300 °C (O_2 mole fractions below 0.05%). At 225 °C, no O_2 was consumed. Without catalyst, the O_2 conversion was below 10% for temperatures below 500 °C. Above 500 °C, the conversion of O_2 increased, reaching complete conversion at 750 °C.

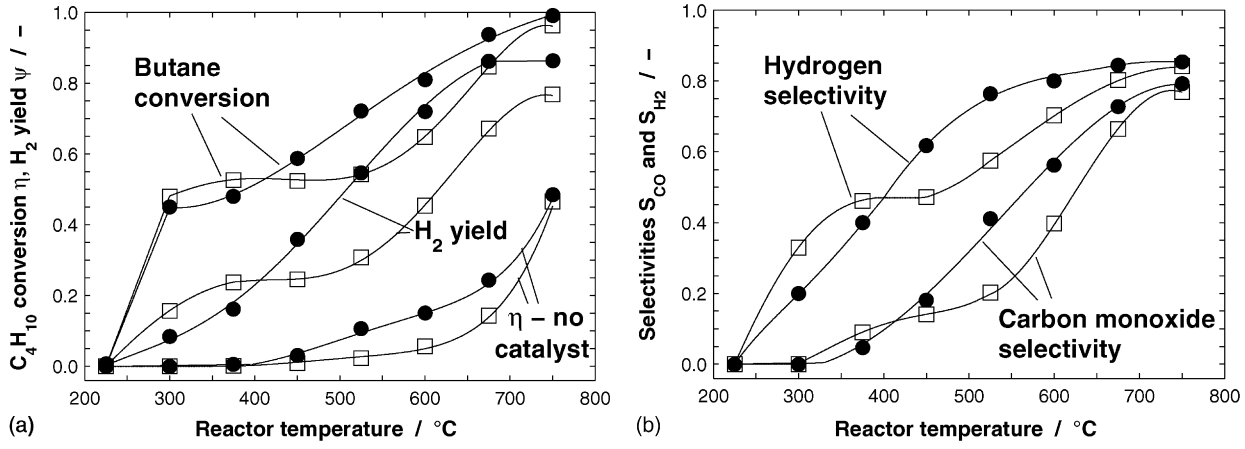

Fig. 4. Butane conversion η and hydrogen yield ψ (a), carbon monoxide selectivity S_{CO} and hydrogen selectivity S_{H_2} (b) as functions of reactor temperature for packed bed reactors with a catalyst loading of 0.5 wt% Rh and for both types of plugs, with SiO_2 (●) and Al_2O_3/SiO_2 (□) fibers, respectively, for an inlet C/O ratio $\phi = 0.8$. The butane conversion is as well shown for a packed bed without catalyst consisting only of SiO_2 sand and both fiber materials. The solid lines through the data points are curve fits.

3.3. Influence of different Rh loadings on the syngas production

The conversion of butane in packed beds consisting of SiO_2 sand, catalyst nanoparticles with Rh loadings from 0 to 2.0 wt% and SiO_2 fiber plugs started below 300 °C. For 0 wt% Rh, the start of butane conversion was delayed compared to packed beds containing Rh. The variation of catalyst loading had no significant influence on the butane conversion η up to 375 °C (Fig. 5a). Between 400 and 600 °C, higher Rh loadings led to remarkably higher butane conversion. For the highest Rh loading of 2.0 wt%, η increased rapidly from 56% at 375 °C to 92% at 525 °C, reaching complete conversion of butane above 600 °C. The difference in conversion for materials with 0.5 and 0.25 wt% Rh was rather small. The addition of 0.1 wt% Rh to the ceria/zirconia had a significant effect on the butane conversion. For 0 wt% Rh, the butane conversion stayed between 41 and 53% from 375 to 750 °C, whereas 0.1 wt% Rh already led to 86% butane conversion at 750 °C.

For all investigated materials containing Rh, the start of butane conversion coincided with the start of H_2 production below 300 °C. For 2.0 wt% Rh, the hydrogen yield ψ increased almost linearly to 86% at 675 °C, staying at this maximum value for higher temperatures (Fig. 5b), and the H_2 selectivity S_{H_2} reached saturation at 86% above 525 °C (Fig. 5d). At temperatures below 400 °C, the Rh loadings of 0.5 and 0.25 wt% showed nearly the same hydrogen yields. On the other hand, for higher temperatures a catalyst with 0.5 wt% Rh allowed a fast rise in H_2 production. Above 600 °C, the addition of more noble metal did not significantly improve the H_2 yield. For 0 wt% Rh, no H_2 was produced at any investigated temperature.

In presence of Rh, the production of CO started later than the conversion of butane and the production of H_2, namely above 350 °C. Above 400 °C, the CO production rose rapidly with large differences in CO selectivity S_{CO} between 500 and 650 °C for different Rh loadings (Fig. 5c). The increase of Rh loading from 0.25 to 0.5 wt% had only a small effect on the CO production. The CO production converged to a maximum of S_{CO} of 83% for all catalyst loadings at 750 °C. Without Rh, a small amount of CO was produced at temperatures above 375 °C leading to a selectivity S_{CO} between 9 and 17%.

As in the case of the previous subsection, no significant amounts of lower hydrocarbons were detected in the off-gases. The mole fractions of lower hydrocarbons were always below 0.05%, except for methane, which was below 0.9%. The C mass balance was closed within 1% and no carbon deposition could be detected optically, indicating the presence of less than

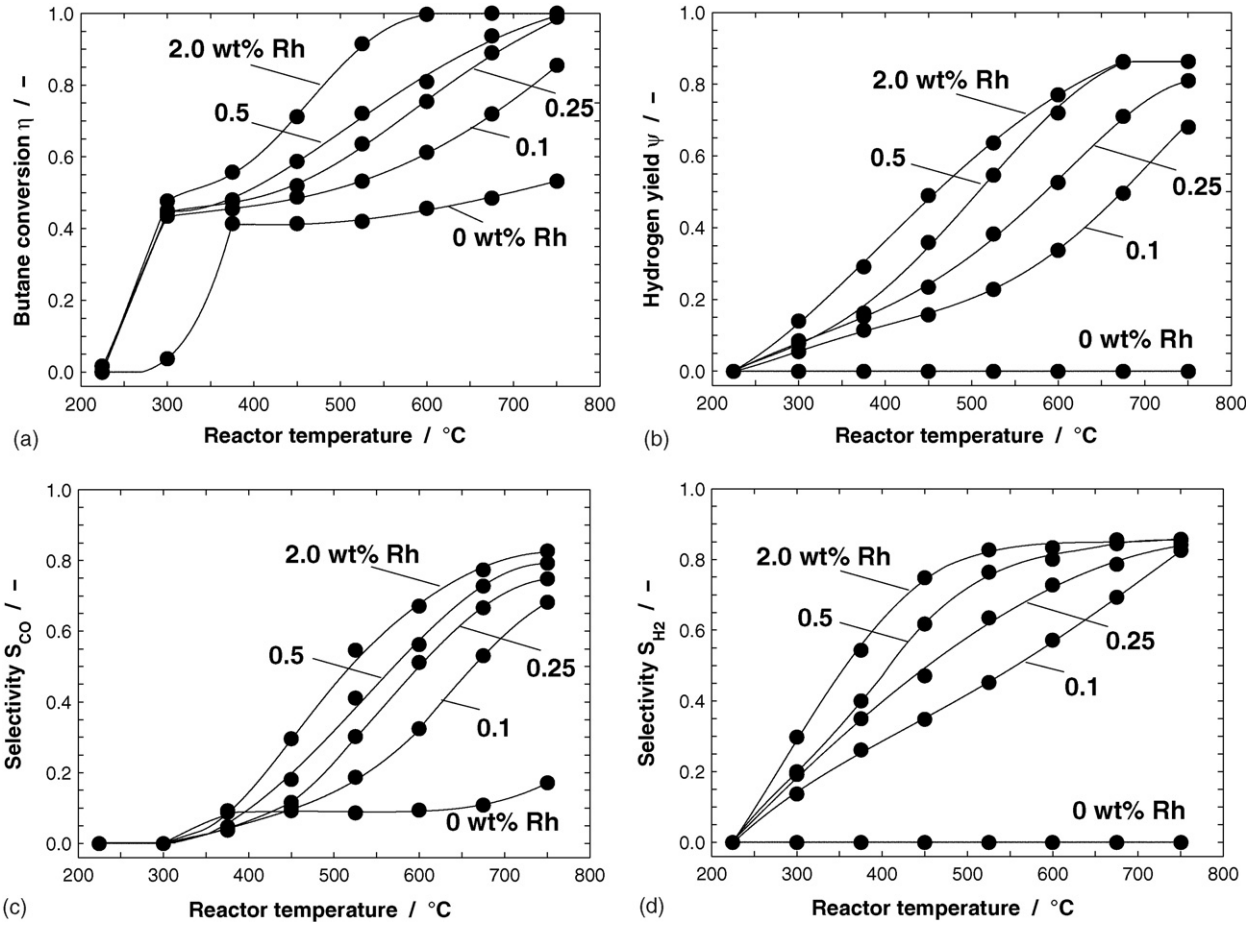

Fig. 5. The influence of Rh loading on $Ce_{0.5}Zr_{0.5}O_2$ on butane conversion η (a), hydrogen yield ψ (b), carbon monoxide selectivity S_{CO} (c), and hydrogen selectivity S_{H_2} (d) for an inlet C/O ratio $\phi = 0.8$, using plugs of SiO_2 fibers. The solid lines through the data points are curve fits.

3.3 mg C per g packed bed material. In addition, measuring the weight of the packed bed did not show any carbon deposition either (detection limit: 0.1 mg).

For reactors with Rh loading, the O_2 conversion ranged from 99 to 100% for temperatures above 300 °C. At 225 °C, no O_2 was consumed. For temperatures above 500 °C, the O_2 mole fraction was always below 0.05% with practically complete O_2 conversion, and for high Rh loading, no O_2 could be detected in the off-gas. Without any Rh loading, hardly any O_2 was converted below 300 °C. Above this temperature, the O_2 conversion reached 95–99%.

4. Discussion

The use of $Rh/Ce_{0.5}Zr_{0.5}O_2$ nanoparticles as catalysts for the partial oxidation (POX) of butane allowed production of H_2 and CO at temperatures as low as 300 °C. While maximum conversion and highest selectivity to H_2 and CO were found at high temperatures, a satisfactory catalytic performance could already be achieved in the present system at relatively low temperatures between 500 and 600 °C. This temperature range was suggested for the incorporation in intermediate-temperature SOFC systems [35,36].

Our more detailed investigation of different reactor materials revealed that the ceramic fiber plugs had a pronounced influence on the overall performance. Fibers consisting of Al_2O_3/SiO_2 resulted in an enhanced butane conversion and H_2/CO production between 300 and 400 °C if compared to pure SiO_2 fibers (Fig. 4). At 400 °C, the performance of a SiO_2 fiber based reactor started to exceed those of Al_2O_3/SiO_2 fibers and grew more evident around 500–650 °C (Table 1). In order to better study this effect, we investigated the chemical reactions in the absence of any noble metal or ceria-based ceramics and used SiO_2-sand filled tubes with ceramic plugs (Fig. 4a). The use of alumina containing fibers significantly reduced the butane conversion by up to a factor of three at 600 °C. A closer view on the corresponding very low amounts of produced H_2 and CO (not shown) indicated that most of the butane is fully oxidized. This clearly illustrated the important contribution of non-noble metal catalyzed butane conversion and possible homogeneous reaction of butane at temperatures above 600 °C. At such high temperature, appreciable amounts of butane were obviously reacting without the need of noble metal activation.

Table 1
Comparison of performance for packed beds with Al_2O_3/SiO_2 and SiO_2 fiber plugs at 525 °C and 600 °C, respectively, using $Rh/Ce_{0.5}Zr_{0.5}O_2$ nanoparticles with 0.5 wt% Rh

	525 °C		600 °C	
	Al_2O_3/SiO_2	SiO_2	Al_2O_3/SiO_2	SiO_2
Butane conversion, η	54%	72%	65%	81%
Hydrogen yield, ψ	31%	55%	45%	72%
H_2 selectivity, S_{H_2}	56%	76%	70%	80%
CO selectivity, S_{CO}	20%	41%	40%	56%
H_2 mole fraction, X_{H_2}	10%	16%	14%	20%
CO mole fraction, X_{CO}	3%	7%	6%	10%

Previous studies suggested that oxidative dehydrogenation and POX of different hydrocarbons are a combination of gas-phase homogeneous and catalyzed heterogeneous reactions [12–20], as mentioned in the first section. The low amount of produced hydrocarbon by-products shown in this study was suggested by [19] as a sign of strong interplay between homogeneous and heterogeneous reactions.

The Rh loading on $Ce_{0.5}Zr_{0.5}O_2$ nanoparticles had an important impact on the production of syngas. However, the Rh loading did not affect all reactions taking place in the reactor in the same way: While the butane conversion η was remarkably higher for an Rh loading of 2.0 wt% compared to 0.5 wt%, the production of H_2 was almost identical above 600 °C for both loadings (Fig. 5). While the H_2 production for 0.5 wt% Rh exceeded significantly the production of H_2 for 0.25 wt%, the difference in butane conversion and CO production was not large for these Rh loadings. These two effects may again be discussed together with results from reactors containing no Rh-based catalyst at all. Figs. 4a and 5a clearly show that the reaction was taking off (light-up) at around 300 °C resulting in a butane conversion independent of the Rh loading (Fig. 5a) or the type of fiber plugs (Fig. 4a). The apparent lack of any effect of increasing Rh catalyst loading can now be compared to the lack of CO selectivity and very low H_2 production at 300 °C. Apparently, a light-off at 300 °C resulted in full oxidation of butane.

The production of H_2 and CO, indicated by their selectivities, differed in their dependence on reactor temperature. For 2.0 wt% Rh loading and SiO_2 fiber plugs, the H_2 selectivity reached half of its maximum value already below 350 °C, whereas the CO selectivity reached this point at around 500 °C. The entire temperature dependent behavior showed much higher H_2 selectivity than CO selectivity. Only above 500–550 °C, the H_2 and CO selectivities had similar values: for a reactor with 2.0 wt% Rh and 600 °C, the value of S_{H_2} was 83% and the value of S_{CO} 67%. At 750 °C, S_{H_2} and S_{CO} amounted to 86% and 83%, respectively. For lower temperatures, the selectivity towards CO was evidently lower compared to that towards H_2: at 450 °C, S_{CO}/S_{H_2} was 40% and at 375 °C, S_{CO}/S_{H_2} equaled only 17%. This strongly suggests that POX was not the only reaction producing H_2, since POX would have led to similar H_2 and CO selectivities. Instead, the reaction was dominated at lower temperatures (below 500 °C) by total oxidation (TOX) of butane followed by H_2O consuming reactions like steam reforming (SR) and water gas shift (WGS). H_2O, which was produced by TOX beside CO_2, reacted with butane by SR to H_2 and CO, where part of this CO reacted subsequently with H_2O by WGS to CO_2 and H_2. This combination of TOX, SR, and WGS explained the stronger H_2 production compared to the CO production, which could not be explained by POX alone. For higher temperatures, POX was the dominating reaction, where H_2 and CO were produced likewise. CO_2 producing reactions like TOX and WGS were unimportant for higher temperatures.

Compared to previous studies on hydrocarbon processors, the catalyst used for this study showed very high syngas production at relatively low temperature. An autothermal

reforming path was investigated by Wang and Gorte for hydrocarbons on Pd/ceria [22], reporting a CO selectivity of 6% and butane conversion of 11% at 450 °C using Pd/ceria as catalyst for SR of butane, compared to a maximum CO selectivity of 30% and butane conversion 71% at the same temperature in the present investigation. At 527 °C, Wang and Gorte [37] achieved butane conversion of 41% by SR on Pd/ceria, in contrast to 92% butane conversion at 525 °C in this study. Acharya et al. [38] investigated SR of isobutane on Pt–CeO_2–Gd_2O_3 and demonstrated butane conversion of 63% and hydrogen yield (as produced hydrogen per hydrogen input from butane and H_2O) of 39% at 600 °C, compared to nearly complete butane conversion and 77% hydrogen yield in this investigation at the same temperature. Huff et al. [10] performed POX of butane over Pt coated foam monoliths with $\phi = 0.9$ resulting in butane conversion of 99%, hydrogen yield of 31%, and CO selectivity of 79% at 1041 °C. In the present study, similar butane conversion and CO selectivity (100% and 77%, respectively) could be obtained at much lower temperature of 675 °C and with a corresponding higher hydrogen yield of 86%. The present investigation on supported Rh catalysts with a very open morphology resulted in higher H_2 and CO yields at lower temperatures compared to other studies, which illustrates the favorable morphological and chemical properties of the aerosol derived ceria/zirconia nanoparticles as a support for Rh. For all measurements, neither significant cracking of butane nor formation of soot could be found, which corresponded well with results from Wang and Gorte [22] and Hilaire et al. [39].

5. Conclusions

The present work investigated the capability of rhodium doped ceria/zirconia nanoparticles as catalysts for the production of syngas from butane at 225–750 °C. The main issue of this study was to develop a high catalytic performance for intermediate temperatures of 500–600 °C. In this range, a packed bed reactor with catalyst nanoparticles of 2.0 wt% Rh loading and SiO_2-based plugs achieved nearly complete butane conversion with a hydrogen yield ψ of 77%. This resulted in an off-gas containing a H_2 mole fraction X_{H_2} of 21% and a CO mole fraction X_{CO} of 13%. In spite of its wide use as a sealing material or monolith base [7–11], the influence of Al_2O_3 in the sealing plugs of the reactor strongly affected the overall performance and suggested a more detailed investigation of non-noble metal catalyzed and homogeneous contributions to butane conversion in such reactors. Our results showed that the here-presented reactor configurations may well be suited to provide small and portable butane processing units for applications together with micro-fuel cells.

Acknowledgements

Financial support for this work provided by KTI/CTI in the context of the OneBat project, Project No. 7085.2 DCPP-NM, and by Swiss Federal Office of Energy (SFOE), Project No. 150563, is gratefully acknowledged. The support from the technical staff of the LTNT (Martin Meuli and Max Hard) was very important for this work.

Appendix A

A.1. Effect of the reactor tube material

All results presented before were conducted for packed beds in an Inconel (Alloy 600) tube due to its easy handling and high robustness. To prove its feasibility as a reactor material in the sense of chemical inertness, reference measurements with the packed beds inside quartz tubes were performed. These results showed no significant effect of the Inconel on the production of syngas. In Fig. 6, characteristic results for two packed beds containing catalytic nanoparticles with 2.0 wt% Rh and SiO_2 fiber plugs inside an Inconel and a quartz tube are compared. Except for a small difference in butane conversion and H_2 production at 300 °C, both reactors showed almost perfect agreement. Therefore, it can be stated that the Inconel tube does

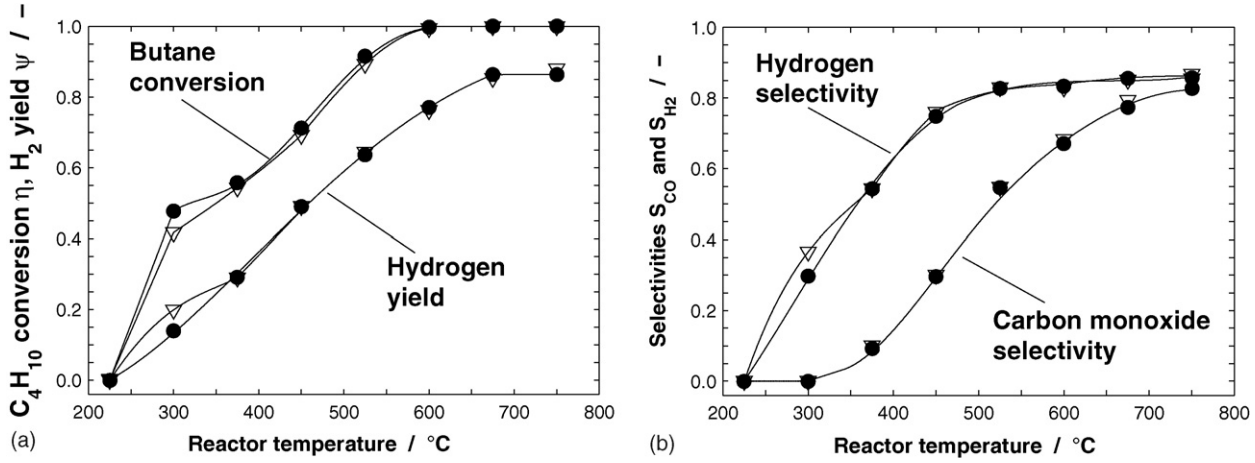

Fig. 6. Butane conversion η and hydrogen yield ψ (a), carbon monoxide selectivity S_{CO} and hydrogen selectivity S_{H_2} (b) as functions of reactor temperature for packed bed reactors with a catalyst loading of 2.0 wt% Rh and SiO_2 fiber plugs in an Inconel reactor tube (●) and a quartz reactor tube (▽), respectively, for an inlet C/O ratio $\phi = 0.8$. The solid lines through the data points are curve fits.

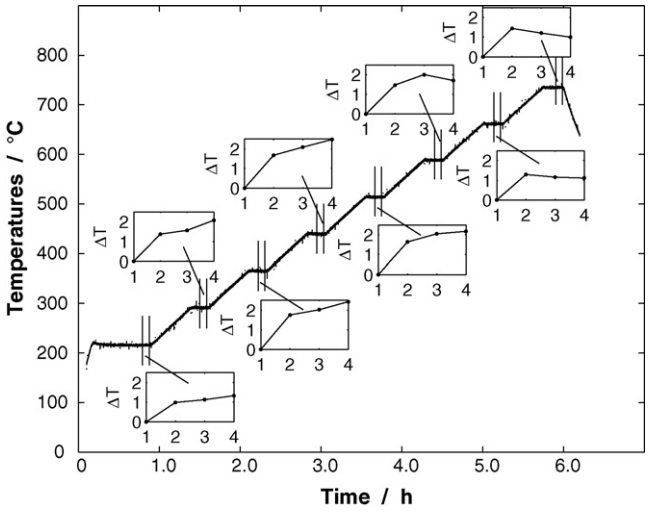

Fig. 7. Temperatures of four thermocouples in the reactor (1: at the inlet, 2 and 3: in the packed bed, 4: at the outlet) during one measurement cycle. The small plots show the four temperatures averaged over 5 min before each measurement point and referenced to the first thermocouple.

not affect the syngas production by $Rh/Ce_{0.5}Zr_{0.5}O_2$ nanoparticles in a significant way for temperatures above 350 °C.

A.2. Temperature profile along the packed bed

For the results presented in this article, isothermal conditions along the packed bed were assumed. To prove that the temperature in the packed bed is identical with the nominal oven temperature and that the temperature variation along the packed bed is negligible, four thermocouples were inserted into the packed bed with about 4 mm distance between each other. The first thermocouple reached the ceramic fiber plug at the inlet of the packed bed. The second and third one were in the packed bed itself. The fourth measured the temperature in the fiber plug at the outlet. In Fig. 7, the four measured temperatures are shown for a typical measuring cycle. It is obvious that the four temperatures only differ very slightly from the nominal oven temperature. The temperature profiles in the packed bed are shown for the eight points where the gas composition was measured, using the temperatures averaged over 5 min before each measurement point and referenced to the first thermocouple. For low oven temperatures, the maximum temperature was reached at the outlet of the packed bed, whereas for higher oven temperatures, the temperature was maximal inside the packed bed. However, the highest temperature variation was always below 2.5 K, corresponding to a relative temperature deviation of less than 0.5%. Therefore, the assumption of isothermal conditions in the packed bed reactor was easily satisfied.

References

[1] N. Hotz, S.M. Senn, D. Poulikakos, J. Power Sources 158 (2006) 333–347.
[2] G.W. Coffey, J.S. Hardy, L.R. Pederson, P.C. Rieke, E.C. Thomsen, Electrochem. Solid State Lett. 1 (2003) A121–A124.
[3] B. Zhu, J. Power Sources 114 (2003) 1–9.
[4] B. Zhu, X.T. Yang, J. Xu, Z.G. Zhu, S.J. Ji, M.T. Sun, J.C. Sun, J. Power Sources 118 (2003) 47–53.
[5] W.J. Stark, K. Wegner, S.E. Pratsinis, A. Baiker, J. Catal. 197 (2001) 182–191.
[6] A. Trovelli, Catalysis by Ceria and Related Materials, Imperial College Press, 2002.
[7] B. Silberova, H.J. Venvik, J.C. Walmsley, A. Holmen, Catal. Today 100 (2005) 457–462.
[8] A. Mitri, D. Neumann, T. Liu, G. Veser, Chem. Eng. Sci. 59 (2004) 5527–5534.
[9] A.S. Bodke, S.S. Bharadwaj, L.D. Schmidt, J. Catal. 79 (1998) 138–149.
[10] M. Huff, P.M. Torniainen, L.D. Schmidt, Catal. Today 21 (1994) 113–128.
[11] D.A. Hickman, L.D. Schmidt, Science 259 (1993) 343–346.
[12] K.T. Nguyen, H.H. Kung, J. Catal. 122 (1990) 415–428.
[13] R. Burch, E.M. Crabb, Appl. Catal. A: Gen. 100 (1993) 111–130.
[14] M. Xu, J.H. Lunsford, React. Kinet. Catal. Lett. 57 (1996) 3–11.
[15] M. Huff, L.D. Schmidt, J. Catal. 149 (1994) 127–141.
[16] A.A. Lemonidou, A.E. Stambouli, Appl. Catal. A: Gen. 171 (1998) 325–332.
[17] K.D. Campbell, E. Morales, J.H. Lunsford, J. Am. Chem. Soc. 109 (1987) 7900–7901.
[18] B. Silberova, H.J. Venvik, A. Holmen, Catal. Today 99 (2005) 69–76.
[19] I. Aartun, B. Silberova, H. Venvik, P. Pfeifer, O. Görke, K. Schubert, A. Holmen, Catal. Today 105 (2005) 469–478.
[20] S. Marengo, P. Comotti, G. Galli, Catal. Today 81 (2003) 205–213.
[21] K. Kunimori, T. Iwade, H. Uetsuka, S. Ito, T. Watanabe, Catal. Lett. 18 (1993) 253–259.
[22] X. Wang, R.J. Gorte, Appl. Catal. A: Gen. 224 (2002) 209–218.
[23] L. Madler, H.K. Kammler, R. Mueller, S.E. Pratsinis, J. Aerosol Sci. 33 (2002) 369–389.
[24] W.J. Stark, L. Madler, M. Maciejewski, S.E. Pratsinis, A. Baiker, Chem. Commun. 5 (2003) 588–589.
[25] M.G. Atwell, J.Y. Hebert, Appl. Spectrosc. 23 (1969) 480–482.
[26] M. Stutz, D. Poulikakos, Chem. Eng. Sci. 60 (2005) 6983–6997.
[27] A. Chaniotis, D. Poulikakos, J. Power Sources 142 (2005) 184–193.
[28] R.E. Hayes, S.T. Kolaczkowski, Introduction to Catalytic Combustion, Taylor & Francis, 1997.
[29] R. Strobel, F. Krumeich, W.J. Stark, S.E. Pratsinis, A. Baiker, J. Catal. 222 (2004) 307–314.
[30] R. Strobel, W.J. Stark, L. Madler, S.E. Pratsinis, A. Baiker, J. Catal. 213 (2003) 296–304.
[31] W.J. Stark, J.D. Grunwaldt, M. Maciejewski, S.E. Pratsinis, A. Baiker, Chem. Mater. 17 (2005) 3352–3358.
[32] H. Kishimoto, T. Omata, S. Otsuka-Yao-Matsuo, K. Ueda, H. Hosono, H. Kawazoe, J. Alloys Compd. 312 (2000) 94–103.
[33] W.J. Stark, M. Maciejewski, L. Madler, S.E. Pratsinis, A. Baiker, J. Catal. 220 (2003) 35–43.
[34] E.A. Kummerle, G. Heger, J. Solid State Chem. 147 (1999) 485–500.
[35] A. Bieberle-Hütter, D. Beckel, U.R. Muecke, J.L.M. Rupp, A. Infortuna, L.J. Gauckler, MST News 4 (2005) 12–15.
[36] B.C.H. Steele, Solid State Ionics 134 (2000) 3–20.
[37] X. Wang, R.J. Gorte, Catal. Lett. 73 (2001) 15–19.
[38] C.K. Acharya, A.M. Lane, T.R. Krause, Catal. Lett. 106 (2006) 41–48.
[39] S. Hilaire, S. Sharma, R.J. Gorte, J.M. Vohs, H.W. Jen, Catal. Lett. 70 (2000) 131–135.